

Quantum dynamics of skyrmions in chiral magnets

Christina Psaroudaki¹, Silas Hoffman¹, Jelena Klinovaja¹, and Daniel Loss¹

¹*Department of Physics, University of Basel, Klingelbergstrasse 82, CH-4056 Basel, Switzerland*

(Dated: December 7, 2016)

We study the quantum propagation of a skyrmion in chiral magnetic insulators by generalizing the micromagnetic equations of motion to a finite temperature path integral formalism, using field theoretic tools. Promoting the center of the skyrmion to a dynamic quantity, the fluctuations around the skyrmionic configuration give rise to a time-dependent damping of the skyrmion motion. From the frequency dependence of the damping kernel, we are able to identify the skyrmion mass, thus providing a microscopic description of the kinematic properties of skyrmions. When the free energy is translationally invariant we find the skyrmion mass is finite only at finite temperature. However, if defects are present or a magnetic trap is applied, the skyrmion mass acquires a finite value, even at vanishingly small temperature. We demonstrate that a skyrmion in a confined geometry provided by a magnetic trap behaves as a massive particle owing to its quasi-one dimensional confinement.

PACS numbers: 75.70.Kw, 75.78.-n, 75.30.+j, 03.70.+k

I. INTRODUCTION

Although skyrmions have been proposed^{1,2} long ago, there has been a strong rise in interest in recent years spurred by experimental observations of skyrmionic phases in various magnetic thin-films³⁻⁵. Magnetic skyrmions are characterized by a topologically nontrivial mapping from a two-dimensional (2D) magnetic system in real space into three-dimensional spin space. This mapping leads to a topological charge Q which characterizes the skyrmion and is given by

$$Q = \frac{1}{4\pi} \int d\mathbf{r} \, \mathbf{m} \cdot (\partial_x \mathbf{m} \times \partial_y \mathbf{m}), \quad (1)$$

where \mathbf{m} is the normalized magnetization vector field and x and y are the spatial coordinates of the 2D magnetic layer^{6,7}. Magnetic skyrmions are attractive candidates for magnetic storage of classical information^{8,9} because they are topologically stable in the sense that no continuous local deformation in the magnetic texture can remove a skyrmion (*i.e.*, change Q), and they can be manipulated at high speed with relatively low current densities^{8,10,11}. Furthermore, because skyrmions coupled to conventional superconductors are known to support Majorana fermions¹², they may be a route to topological quantum computation¹³.

The dynamics of any classical magnetic texture with fixed magnitude, \mathbf{m} , is governed by the Landau-Lifshitz-Gilbert (LLG) equation^{14,15}. The dynamic properties of skyrmions can be considerably simplified by considering the motion of the average magnetic texture¹⁶, which reduces to an equation of motion for the skyrmion's center-of-mass coordinate, known as Thiele's equation. This skyrmion coordinate behaves as a massless Dirac-like particle under a Magnus force proportional to Q ¹⁷, and a possible damping is parameterized by a phenomenological velocity-dependent term that is induced by the coupling of the skyrmion motion to other degrees of freedom in the system such as electrons, phonons, magnons, etc.; the microscopic details of this coupling are typically left unspecified. Using this phenomenological approach, several generalized equations have been proposed¹⁸⁻²¹ for a rigid magnetic structure in the presence of external static as well as rapidly changing forces. The thermal diffusion

of a driven skyrmion has been studied within the classical framework by a numerical solution of the stochastic LLG equation¹⁸, where random fields are included to model the effects of thermal fluctuations.

However, for small skyrmions at the nanometer scale, the size of skyrmions in state-of-the-art experiments²²⁻²⁵, quantum fluctuations are expected to become relevant²⁶ and the classical LLG equation is expected to break down. In a fully quantum mechanical treatment starting from the spin and other degrees of freedom present in the system the quantum dynamics of the skyrmion should emerge naturally, giving rise for instance to possible mass and dissipation terms linked to the underlying microscopics.

The goal of this work is to provide such a quantum treatment of skyrmions in insulating magnetic films. Thereby we will restrict ourselves to systems where only spin degrees of freedom are present and other sources such as phonons and itinerant electrons are assumed to be negligibly small (due to low enough temperatures) or entirely absent, respectively. By employing quantum field theory methods and the Fadeev-Popov techniques for collective coordinates²⁷⁻³⁰, applied to magnetic systems^{31,32}, we will derive the quantum dynamics of the skyrmion in a systematic way, thereby going beyond the classical limit.

Within this formalism the skyrmion position, which parametrizes the classical static solution of the Euler-Lagrange equations, is promoted to a time-dependent dynamical variable and a finite perturbation theory in terms of fluctuations around the skyrmion configuration is performed. The interaction of the skyrmion with these magnon modes gives rise to dissipation and to a non-local damping kernel whose form we obtain in a closed form and can evaluate analytically in some regimes of physical interest. In particular, we are able to microscopically calculate the contribution to the damping in the Thiele equation from the incoherent magnon modes which in general depends on the magnetic dispersion relation and thus on the details of the free energy of the system.

For asymptotic (imaginary) times, we find that the damping kernel becomes local in time and reduces to a simple mass term which we can calculate explicitly in the presence of non-uniform magnetic traps and spatially dependent exchange in-

interactions for arbitrary temperatures. Specifically, in the zero-temperature limit we find that local defects and magnetic traps which break translational symmetry induce a finite mass so that the skyrmion motion is no longer Dirac-like but rather follows a quadratic dispersion law of a massive particle. As a striking consequence, we find that in quasi-one dimensional wire geometries the skyrmion acquires a finite mass. Such geometries are provided for instance by anisotropic magnetic traps, similar to linear tracks used for magnetic memory and logic devices^{8,33,34}. Surprisingly, this shows that skyrmions in quantum confined geometries exhibit a fundamentally different dynamical behaviour compared to the one in unconfined geometries.

The paper is organized as follows. In Sec. II we derive a coherent-state path integral for a generic magnetic texture, while in Sec. III, we utilize this functional integral approach to calculate the damping experienced by such a magnetic texture as a result of the coupling to magnon fluctuations, and we also demonstrate that this damping reduces to a simple mass term. In Sec. IV, we apply our formalism to a chiral magnet and show in Sec. V, that only a spatially nonuniform perturbation to the magnetic texture induces a skyrmion mass at zero temperature. To complete the description we examine in Sec. VI the skyrmion mass at finite temperatures. We conclude with a discussion and some general remarks in Sec. VII and Sec. VIII. Technical details are deferred to several appendices.

II. COLLECTIVE COORDINATE QUANTIZATION

We consider a thin magnetic insulator with normalized magnetization $\mathbf{m}(\tilde{\mathbf{r}}) = (\sin \Theta(\tilde{\mathbf{r}}) \cos \Phi(\tilde{\mathbf{r}}), \sin \Theta(\tilde{\mathbf{r}}) \sin \Phi(\tilde{\mathbf{r}}), \cos \Theta(\tilde{\mathbf{r}}))$ in polar coordinates, where the z axis points along the smallest dimension of the magnet (for the connection to spins in a 2D lattice model, see below). For sufficiently thin magnets, *i.e.*, thinner than the exchange length, the magnetization is constant along the z axis and $\tilde{\mathbf{r}} = (\tilde{\rho} \cos \phi, \tilde{\rho} \sin \phi)$ is a vector in the xy plane. The Lagrangian of such a magnetic system is given by

$$L = \frac{SN_A}{\alpha^2} \int d\tilde{\mathbf{r}} \dot{\Phi}(1 - \Pi) + N_A \int d\tilde{\mathbf{r}} \mathcal{F}(\Phi, \Pi), \quad (2)$$

where S is the magnitude of the spin, N_A is the number of magnetic layers along the z axis, α is the lattice spacing, $\dot{\Phi}$ is the time derivative of $\Phi(\tilde{\mathbf{r}}, t)$ and $\Pi(\tilde{\mathbf{r}}, t) \equiv \cos \Theta$ is canonically conjugate to Φ . The first term in Eq. (2), *i.e.*, the Wess-Zumino or Berry phase contribution (using the north pole parametrization³¹), describes the dynamics of the magnetization while the second term is the free energy which, in this and the following section, we keep general. For reasons of simplicity we assume that the energy density functional $\mathcal{F}(\Phi, \Pi)$ is translationally invariant whereas the rotational invariance is broken. Upon minimizing L , one recovers the Euler-Lagrange or, equivalently, the Landau-Lifshitz (LL) equations, which govern the classical motion of the magnetization $\mathbf{m}(\tilde{\mathbf{r}}, t)$.

To investigate the quantum effects of such a magnetic texture, we employ a functional integral formulation in which the partition function is given by $Z = \int \mathcal{D}\Pi \mathcal{D}\Phi e^{-S_E}$, where $S_E = \int_0^{\tilde{\beta}} d\tilde{\tau} \mathcal{L}$ is the Euclidean action. Here, \mathcal{L} is the imaginary time Lagrangian, which is obtained upon replacing time t with imaginary time $\tilde{\tau} = it$, and where $\tilde{\beta} = 1/k_B \tilde{T}$ for the system temperature \tilde{T} with k_B the Boltzmann constant. Throughout this work we assume that $\hbar = 1$. We also introduce dimensionless variables $\mathbf{r} = \tilde{\mathbf{r}}/l\alpha$, $\tau = \tilde{\tau}\varepsilon_\Lambda$, and $\beta = \tilde{\beta}\varepsilon_\Lambda$. Here l , a dimensionless constant, and ε_Λ , a characteristic energy scale, depend on the system under study and will be specified later in Sec. IV. With increasing number of layers the effective spin $N_A S$ of the texture increases, and thereby $\mathbf{m}(\mathbf{r}, \tau)$ approaches a macroscopic description of a classical magnetization field. We therefore consider the limit $N_A \gg 1$ to capture the leading semiclassical effects.

Henceforth, we consider a specific class of free energies which furnish a static stable or metastable solution, $\mathbf{m}_0(\mathbf{r}) = [\sin \Theta_0(\mathbf{r}) \cos \Phi_0(\mathbf{r}), \sin \Theta_0(\mathbf{r}) \sin \Phi_0(\mathbf{r}), \cos \Theta_0(\mathbf{r})]$, in which \mathbf{m}_0 is characterized by a topological number Q and the magnetization profile Θ_0 approaches a constant value at spatial infinity $|\mathbf{r}| \rightarrow \infty$. We refer to these textures as skyrmions and an explicit solution will be discussed later in detail. First, we develop a formalism which is valid for general solutions.

The center-of-mass of such solutions $\mathbf{m}_0(\mathbf{r})$ is denoted by the collective coordinate $\mathbf{R}(\tau)$, which is energy-independent owing to the translational symmetry of the system. The dynamics of the skyrmion is then described by $\mathbf{R}(\tau)$ and the magnetization fluctuations which arise when the skyrmion moves. Due to the non-linear character of the LL equation these fluctuations couple back to $\mathbf{R}(\tau)$ and thus affect the skyrmion motion. To describe this effect we perform a canonical transformation of the path integral variables which separates the collective coordinate $\mathbf{R}(\tau)$ from the fluctuations around the skyrmion^{27,28},

$$\begin{aligned} \Pi(\mathbf{r}, \tau) &= \Pi_0(\mathbf{r} - \mathbf{R}) + \eta(\mathbf{r} - \mathbf{R}, \tau), \\ \Phi(\mathbf{r}, \tau) &= \Phi_0(\mathbf{r} - \mathbf{R}) + \xi(\mathbf{r} - \mathbf{R}, \tau). \end{aligned} \quad (3)$$

In the presence of translational symmetry there is a degenerate pair of zero-frequency modes $\xi \propto \partial_i \Phi$ and $\eta \propto \partial_i \Pi$, associated with translation of the skyrmion position in the $i = x, y$ direction. Instead of fluctuations ξ and η , it is more convenient to work with the spinors χ and χ^\dagger defined by

$$\chi = \frac{1}{2} \begin{pmatrix} \xi \sin \Theta_0 + i\eta / \sin \Theta_0 \\ \xi \sin \Theta_0 - i\eta / \sin \Theta_0 \end{pmatrix}. \quad (4)$$

We denote as \mathcal{Y}_x and \mathcal{Y}_y the degenerate pair of translational zero-modes expressed in the spinor notation of Eq. (4). We now construct a finite perturbation theory in terms of fluctuations around $\mathbf{m}_0(\mathbf{r} - \mathbf{R})$, where the system is described from a translated spatial frame $\tilde{\mathbf{r}} = \mathbf{r} - \mathbf{R}(\tau)$. To second order in χ , the action $S_E = S_{\text{cl}} + S_{\text{fl}} + S_I$ separates into three parts. The first part describes the translational motion of \mathbf{m}_0 ,

$$S_{\text{cl}} = -i\tilde{S}N_A \int_0^\beta d\tau \int d\tilde{\mathbf{r}} \dot{\mathbf{R}} \cdot (1 - \Pi_0) \nabla \Phi_0, \quad (5)$$

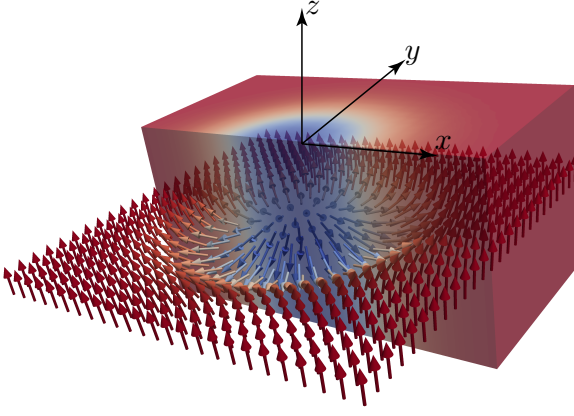


FIG. 1. (color online). Illustration of a magnetic layer hosting a skyrmion with topological number $Q = 1$ embedded in a bulk magnetic insulator. The magnetization $\mathbf{m}(\bar{\mathbf{r}})$ is assumed to be uniform along the direction perpendicular to the layer.

where $\tilde{S} = Sl^2$ and where we have ignored an overall constant from the configuration energy $(l\alpha)^2 \int d\bar{\mathbf{r}} \mathcal{F}(\Phi_0, \Pi_0)$. The second part consists of the fluctuations $\chi(\bar{\mathbf{r}}, \tau)$ around $\mathbf{m}_0(\bar{\mathbf{r}})$, which we can consider as spin waves or magnons, given by

$$S_{\text{fl}} = N_A \chi^\dagger \cdot \mathcal{G} \chi. \quad (6)$$

Here we introduced the compact scalar product notation for operators and functions,

$$\chi^\dagger \cdot \mathcal{G} \chi \equiv \int d\tau d\tau' d\bar{\mathbf{r}} d\bar{\mathbf{r}}' \chi^\dagger(\bar{\mathbf{r}}, \tau) \mathcal{G}(\bar{\mathbf{r}}, \tau; \bar{\mathbf{r}}', \tau') \chi(\bar{\mathbf{r}}', \tau'), \quad (7)$$

where the scalar product in spinor space is left implicit. Further we defined

$$\begin{aligned} \mathcal{G} &= \tilde{S} \sigma_z \partial_\tau + \mathcal{H}, \\ \mathcal{H} &= \frac{(l\alpha)^2}{\varepsilon_A} \delta_{\chi^\dagger} \delta_{\chi} \mathcal{F}|_{\chi=\chi^\dagger=0}, \end{aligned} \quad (8)$$

where δ_{χ} is the functional derivative with respect to the field $\chi(\bar{\mathbf{r}}, \tau)$, and \mathcal{G} is the magnon Green's function. Finally, the coupling between the center-of-mass $\mathbf{R}(\tau)$ and the spin waves $\chi(\bar{\mathbf{r}}, \tau)$ is given by

$$S_I = N_A (\chi^\dagger \cdot \mathcal{K} \chi + \mathcal{J}^\dagger \cdot \chi + \chi^\dagger \cdot \mathcal{J}), \quad (9)$$

where

$$\begin{aligned} \mathcal{K} &= -\tilde{S} \sigma_z \dot{\mathbf{R}}_i \Gamma_i, \\ \mathcal{J} &= -\tilde{S} \sigma_z \dot{\mathbf{R}}_i f_i. \end{aligned} \quad (10)$$

Here, repeated indices, $i, j = x, y$, are summed over and we introduced the abbreviations

$$\begin{aligned} \Gamma_i &= \partial_i - \sigma_x \cot \Theta_0 \partial_i \Theta_0, \\ f_i &= \frac{1}{2} \begin{pmatrix} \sin \Theta_0 \partial_i \Phi_0 - i \partial_i \Theta_0 \\ \sin \Theta_0 \partial_i \Phi_0 + i \partial_i \Theta_0 \end{pmatrix}. \end{aligned} \quad (11)$$

Because the translational modes have already been accounted for in $\mathbf{R}(\tau)$, they must be explicitly excluded from the integration over χ and χ^\dagger to avoid overcounting of degrees of freedom. For this we require $G_i = \int d\bar{\mathbf{r}} \chi^\dagger(\bar{\mathbf{r}}) \mathcal{Y}_i(\bar{\mathbf{r}}) = 0$ and implement this constraint by means of the Faddeev-Popov (FP) technique^{29,30} by inserting a factor of unity $1 = \int d\mathbf{R}(\tau) \det(J_{\mathbf{G}}) \delta(G_x) \delta(G_y)$ into the partition function, where $\delta(\cdot)$ is the Dirac delta function. We then obtain

$$\begin{aligned} Z &= \int d\mathbf{R} e^{-S_{\text{cl}}} \tilde{Z}[\mathbf{R}], \\ \tilde{Z} &= \int d\chi^\dagger d\chi \delta(G_x) \delta(G_y) \det(J_{\mathbf{G}}) e^{-S_{\text{fl}} - S_I}, \end{aligned} \quad (12)$$

where $J_{\mathbf{G}} = d\mathbf{G}(\tau)/d\mathbf{R}(\tau')$ is the Jacobian of the coordinate transformation and is treated as an additional term in the action, adaptable for perturbative calculation. We should stress that the scalar product $\chi^\dagger(\bar{\mathbf{r}}) \mathcal{Y}_i(\bar{\mathbf{r}})$ (in the 2-spinor space) is determined by the properties of the Hamiltonian \mathcal{H} . In most cases \mathcal{H} is not Hermitian for the standard metric and orthogonality conditions are enforced by an inner product of the form $\chi^\dagger(\bar{\mathbf{r}}) \sigma_z \mathcal{Y}_i(\bar{\mathbf{r}})$ ³⁵.

We next integrate out the fluctuations χ and χ^\dagger from the partition function neglecting terms $O(1)$ in N_A which originate from the FP determinant $\det(J_{\mathbf{G}})$. The integral over χ and χ^\dagger can be reduced to a Gaussian form by completing the square, $\tilde{\chi} = \chi + (\mathcal{G} + \mathcal{K})^{-1} \mathcal{J}$. The inverse of an operator, O^{-1} , is defined by $\int d\bar{\mathbf{r}}'' d\tau'' O(\bar{\mathbf{r}}, \tau; \bar{\mathbf{r}}'', \tau'') O^{-1}(\bar{\mathbf{r}}'', \tau''; \bar{\mathbf{r}}', \tau') = \delta(\bar{\mathbf{r}} - \bar{\mathbf{r}}') \delta(\tau - \tau')$. After integration, the partition function reduces to

$$\begin{aligned} \tilde{Z}[\mathbf{R}] &= \int d\tilde{\chi}^\dagger d\tilde{\chi} \delta(G_x) \delta(G_y) e^{-\mathcal{I} - N_A \tilde{\chi}^\dagger \cdot (\mathcal{G} + \mathcal{K}) \tilde{\chi}} \\ &= e^{-\mathcal{I}} \frac{1}{\det'[N_A(\mathcal{G} + \mathcal{K})]}, \end{aligned} \quad (13)$$

where the prime on the determinant excludes the zero modes, and where

$$\begin{aligned} \mathcal{I} &= -N_A \mathcal{J}^\dagger \cdot (\mathcal{G} + \mathcal{K})^{-1} \mathcal{J} \\ &\approx -N_A \mathcal{J}^\dagger \cdot \mathcal{G}^{-1} \mathcal{J}. \end{aligned} \quad (14)$$

Upon exponentiating the determinant and expanding to lowest nonvanishing order in $\dot{\mathbf{R}}$, we get

$$\frac{1}{\det'[N_A(\mathcal{G} + \mathcal{K})]} \approx \frac{e^{-\text{Tr}'[-\frac{1}{2}(\mathcal{G}^{-1}\mathcal{K})^2]}}{\det'(N_A\mathcal{G})}, \quad (15)$$

where $\text{Tr}' O = \int d\tau d\bar{\mathbf{r}} O(\bar{\mathbf{r}}, \tau; \bar{\mathbf{r}}, \tau)$ denotes the trace and where we have used that $\text{Tr}'(\mathcal{G}^{-1}\mathcal{K}) = 0$ due to periodic boundary conditions in time. The approximations in Eq. (14) and Eq. (15) neglect terms $\mathcal{O}(\dot{\mathbf{R}}^3)$.

III. SKYRMION MASS AND DISSIPATION

Because $\tilde{Z}[\mathbf{R}]$ is, in general, nonlocal in time, it naturally encodes dissipation of the skyrmion that is captured by the

action

$$S_d = -N_A \mathcal{J}^\dagger \cdot \mathcal{G}^{-1} \mathcal{J} - \text{Tr}' \left[\frac{1}{2} (\mathcal{G}^{-1} \mathcal{K})^2 \right]. \quad (16)$$

Let $\Psi_n(\mathbf{r}) e^{i\omega_\nu \tau} / \sqrt{\beta}$ be the normalized eigenvectors of the operator \mathcal{G} ,

$$\mathcal{G} \Psi_n(\mathbf{r}) e^{i\omega_\nu \tau} = (\tilde{S} i\omega_\nu + 2\varepsilon_n) \sigma_z \Psi_n(\mathbf{r}) e^{i\omega_\nu \tau}, \quad (17)$$

where $\omega_\nu = 2\pi\nu/\beta$ are the Matsubara frequencies, with ν integer, and where ε_n is the corresponding eigenenergy of the magnons, given as solutions of the eigenvalue problem $\mathcal{H} \Psi_n = 2\varepsilon_n \sigma_z \Psi_n$. Using this complete basis we get

$$\mathcal{G}^{-1}(\mathbf{r}, \tau; \mathbf{r}', \tau') = \frac{1}{\beta} \sum_{i\omega_\nu, n} \frac{\sigma_z \Psi_n(\mathbf{r}) \Psi_n^\dagger(\mathbf{r}') e^{i\omega_\nu(\tau-\tau') \sigma_z}}{\tilde{S} i\omega_\nu + 2\varepsilon_n}. \quad (18)$$

Insertion of the series expression (18) into Eq. (16) yields

$$S_d = \int_0^\beta d\tau \int_0^\beta d\sigma \dot{R}_i(\tau) \gamma_{ij}(\tau - \sigma) \dot{R}_j(\sigma), \quad (19)$$

where summation over repeated indices $i, j = x, y$ is implied. The damping kernel $\gamma_{ij} = \gamma_{ij}^0 + \gamma_{ij}^T$ consists of a term proportional to the effective spin $N_A S$,

$$\gamma_{ij}^0(\tau) = \frac{1}{\beta} \sum_{i\omega_\nu} \sum_n' \frac{\mathcal{A}_{ij}^n e^{i\omega_\nu \tau}}{i\omega_\nu + \tilde{\varepsilon}_n}, \quad (20)$$

where $\tilde{\varepsilon}_n = 2\varepsilon_n/\tilde{S}$, the prime in the sum denotes omission of the zero modes, and the elements \mathcal{A}_{ij}^n are given by

$$\mathcal{A}_{ij}^n = \tilde{S} N_A \langle f_i, \Psi_n \rangle \langle \Psi_n, f_j \rangle. \quad (21)$$

Here, we have introduced the notation $\langle f, g \rangle = \int d\mathbf{r} f^\dagger(\mathbf{r}) g(\mathbf{r})$. The second part of the kernel is calculated by evaluating the trace in Eq. (16) in the eigenbasis of the operator \mathcal{G} ,

$$\gamma_{ij}^T(\tau) = \frac{1}{\beta^2} \sum_{i\omega_\nu, i\omega_{\nu'}, n, n'}' \frac{\mathcal{B}_{ij}^{n, n'} e^{i(\omega_\nu - \omega_{\nu'}) \tau}}{(i\omega_\nu + \tilde{\varepsilon}_n)(i\omega_{\nu'} + \tilde{\varepsilon}_{n'})}, \quad (22)$$

with matrix elements

$$\mathcal{B}_{ij}^{n, n'} = \frac{1}{2} \langle \Psi_n, \sigma_z \Gamma_i \Psi_{n'} \rangle \langle \Psi_{n'}, \Gamma_j \sigma_z \Psi_n \rangle. \quad (23)$$

The sums (20) and (22) over Matsubara frequencies ω_ν can be explicitly performed using the following exact relation,

$$\frac{1}{\beta} \sum_\nu \frac{e^{i\omega_\nu \tau}}{\omega_\nu^2 + \varepsilon_n^2} = \frac{1}{2\varepsilon_n} \frac{\cosh(\varepsilon_n(|\tau| - \beta/2))}{\sinh(\beta\varepsilon_n/2)} \quad (24)$$

where the RHS is understood to be periodically extended beyond $|\tau| \leq \beta/2$. However, for the purposes considered here it is sufficient to note that the damping $\gamma_{ij}(\tau)$ depends on the modulus of imaginary time $\gamma_{ij}(\tau) = \gamma_{ij}(|\tau|)$. This implies that only the part symmetric in the indices $i, j = x, y$ of the

off-diagonal terms survive in Eq. (19), and thus we can assume $\gamma_{xy} = \gamma_{yx}$ and ignore any antisymmetric contribution.

The action Eq. (19) takes the typical form of a system coupled to a thermal reservoir governed by a linear dissipative process³⁶. The expression for S_d contains contributions that are nonlocal in imaginary time and describe effective correlations of R_i with itself at different times. These correlations are a consequence of an emission of a virtual magnon at time τ generated by the motion of the skyrmion which is then reabsorbed by the skyrmion at a later time τ' . The contributions at equal times, if finite, will give rise to a mass of the skyrmion, which otherwise is absent. The form of the kernel γ_{ij} obviously depends on the microscopic details of the system and determines the amplitude of these effects as we will see below.

For the case of a translationally invariant free energy, the translational modes with zero energy are proportional to the functions f_i . Because the summation over the magnon modes excludes translation, $\mathcal{A}_{ij}^0 = 0$, we conclude that there is no mass contribution from the damping kernel γ_{ij}^0 . This is in agreement with the well-known result that the skyrmion behaves like a massless Dirac particle¹⁶. However, the situation changes if we allow for a perturbation in our free energy, denoted by $\mathcal{V}(\mathbf{r})$, which explicitly breaks translational symmetry. Treating $\mathcal{V}(\mathbf{r})$ in standard perturbation theory, the magnon states become in lowest order,

$$\tilde{\Psi}_n(\mathbf{r}) = \Psi_n(\mathbf{r}) + \sum_{m \neq n} \frac{\Psi_m(\mathbf{r})}{\varepsilon_n^0 - \varepsilon_m^0} \langle \Psi_m, \mathcal{W} \Psi_n \rangle, \quad (25)$$

where $\mathcal{W} = \delta_{\chi^\dagger} \delta_{\chi} \mathcal{V}|_{\chi=\chi^\dagger=0}$. Using the orthogonality properties of the unperturbed magnon modes, we find to lowest order in $\mathcal{V}(\mathbf{r})$,

$$\mathcal{A}_{ij}^n = \frac{\tilde{S} N_A}{(\varepsilon_n^0)^2} \langle f_i, \sigma_z \mathcal{W} \Psi_n \rangle \langle \Psi_n, \mathcal{W} \sigma_z f_j \rangle, \quad (26)$$

which in general is non-zero (see below).

In contrast to γ_{ij}^0 , the finite-temperature contribution to dissipation, γ_{ij}^T , assumes a finite value in general, *i.e.*, we find non-zero matrix elements $\mathcal{B}_{ij}^{n, n'} \neq 0$, even for a translationally invariant system.

The first variation of the action $S_{cl} + S_d$ vanishes for the extremal (classical) path $R_i(\tau)$ obeying the following equation of motion in bosonic Matsubara ω_ν frequency space,

$$\tilde{Q} \omega_\nu \epsilon_{ij} R_j^{\omega_\nu} + 2\omega_\nu^2 \gamma_{ij}^{\omega_\nu} R_j^{\omega_\nu} = -V_i^{\omega_\nu}, \quad (27)$$

where ϵ_{ij} is the Levi-Civita tensor and summation over repeated indices i, j is implied. Here, the β -periodic functions in imaginary time are expanded into Fourier series as

$$R_i(\tau) = \frac{1}{\beta} \sum_{i\omega_\nu} e^{i\omega_\nu \tau} R_i^{\omega_\nu}, \quad (28)$$

and we have also assumed the presence of a potential term \mathcal{V} which breaks translational symmetry which is incorporated in the equation of motion through

$$V_i^{\omega_\nu} = \int_0^\beta d\tau e^{-i\omega_\nu \tau} \frac{\delta \mathcal{V}}{\delta R_i}. \quad (29)$$

TABLE I. Reduced Units

Length	Imaginary Time	Inverse Temperature	Temperature	Magnetic Field	Easy-axis Anisotropy
$\tilde{\mathbf{r}} = \mathbf{r} \frac{\tilde{J}_D}{D}$	$\tilde{\tau} = \tau \frac{1}{JS^2}^a$	$\tilde{\beta} = \beta \frac{1}{JS^2}$	$\tilde{T} = T \frac{JS^2}{k_B}$	$g\mu_B \tilde{H} = h \frac{D^2}{J}$	$\tilde{K} = \kappa \frac{D^2}{J}$

^a $\hbar = 1$

The first term in (27) originates from the Berry phase and results in a Magnus force acting on the skyrmion proportional to the winding number $\tilde{Q} = 4\pi\tilde{S}N_AQ$, recovering well-known results^{16,17}. The Fourier coefficients $\gamma_{ij}^{\omega_\nu}$ are found from Eqs. (20) and (22),

$$\gamma_{ij}^{\omega_\nu} = \sum_n' \frac{\mathcal{A}_{ij}^n}{i\omega_\nu + \tilde{\varepsilon}_n} + \sum_{n,n'}' \frac{\mathcal{B}_{ij}^{n,n'}}{2} \frac{\coth(\frac{\beta\tilde{\varepsilon}_n}{2}) - \coth(\frac{\beta\tilde{\varepsilon}_{n'}}{2})}{\tilde{\varepsilon}_{n'} - \tilde{\varepsilon}_n + i\omega_\nu}. \quad (30)$$

The quantum dynamics of the skyrmion is described by a kernel $\gamma_{ij}^{\omega_\nu}$ with a strong frequency-dependence, in contrast to the typical Gilbert damping. Strongly frequency-dependent dynamics was also predicted for the skyrmion motion in the presence of random time-dependent thermal forces, through a numerical solution of the stochastic LLG equation¹⁸. For asymptotic imaginary times $\tau \gg \varepsilon_{\text{gap}}^{-1}$, *i.e.*, $i\omega_\nu \ll \varepsilon_{\text{gap}}^{-1}$, where ε_{gap} is the lowest magnon energy gap, the effect of the damping can be reduced to a mass term³². From equations (27) and (30), we define the mass tensor as $\mathcal{M}_{ij} = \gamma_{ij}(i\omega_\nu \rightarrow 0)$ with

$$\mathcal{M}_{ij} = \mathcal{M}_{ij}^0 + \mathcal{M}_{ij}^T, \quad (31)$$

where the first term is temperature-independent and given by

$$\mathcal{M}_{ij}^0 = \sum_n' \frac{2\mathcal{A}_{ij}^n}{\tilde{\varepsilon}_n}, \quad (32)$$

while the second mass term is explicitly temperature dependent,

$$\mathcal{M}_{ij}^T = \sum_{\substack{n,n' \\ \tilde{\varepsilon}_n \neq \tilde{\varepsilon}_{n'}}} \frac{\mathcal{B}_{ij}^{n,n'} [\coth(\frac{\beta\tilde{\varepsilon}_{n'}}{2}) - \coth(\frac{\beta\tilde{\varepsilon}_n}{2})]}{\tilde{\varepsilon}_n - \tilde{\varepsilon}_{n'}} + \sum_{\substack{n,n' \\ \tilde{\varepsilon}_n = \tilde{\varepsilon}_{n'}}} \frac{\beta \mathcal{B}_{ij}^{n,n'}}{2 \sinh^2(\beta\tilde{\varepsilon}_n/2)} \quad (33)$$

and vanishes at zero-temperature. The definition of the mass as the zero-frequency limit of the damping kernel $\gamma_{ij}(i\omega_\nu)$ is valid under the assumption that the real-time dynamics of the skyrmion is described by circular modes $\tilde{\omega}$ that are small compared to the magnon gap $\tilde{\omega} \ll \varepsilon_{\text{gap}}$. For example, in the presence of a parabolic potential well $\mathcal{V} = K(R_x^2 + R_y^2)/2$, the characteristic frequency of the circular motion in the absence of a mass is $\tilde{\omega} = K/\tilde{Q}$. Here, \mathcal{V} is a perturbation to the magnon Hamiltonian \mathcal{H} and \tilde{Q} is proportional to the effective spin N_AS , thus the $i\omega_\nu \rightarrow 0$ limit in the mass definition is well

justified. In the opposite case of a large dominant frequency, the mass tensor is refined around $\tilde{\omega}$ as $\mathcal{M}_{ij} = \gamma_{ij}(i\omega \rightarrow \tilde{\omega})$.

The equation of motion Eq. (27) and the mass tensor Eq. (31) are the main results of this section. They are valid for a general magnetic texture $\mathbf{m}(\mathbf{r}, \tau)$ satisfying the specified requirements, and govern the dynamics of its center-of-mass position $\mathbf{R}(\tau)$, taking into account quantum and thermal fluctuations and allowing for a potential \mathcal{V} that weakly breaks the translational symmetry. This equation includes only dissipation produced by the magnon modes, while other sources giving rise to damping such as phonons and itinerant electrons are not included. Thus, we also must assume that we work at low enough temperatures such that phonon effects can be safely neglected. It is worth mentioning that additional forces should be included in Eq. (27) in the presence of a constant magnon current generated by a source³⁷ or by a magnon current induced by a temperature gradient³⁸.

The presence of a non-negligible mass term leads to additional oscillatory modes in the real-time dynamics of the skyrmion^{19,39}. From the structure of elements \mathcal{A}_{ij}^n of Eq. (21) and $\mathcal{B}_{ij}^{n,n'}$ of Eq. (23), it is easy to see that in the presence of a nonuniform but isotropic potential \mathcal{V} or at finite T , diagonal mass elements are equal, $\mathcal{M}_{xx} = \mathcal{M}_{yy}$, and off-diagonal terms are antisymmetric $\mathcal{M}_{xy} = -\mathcal{M}_{yx}$ and will not contribute to the equation of motion. Therefore, in the absence of a driving force and assuming that the confinement is given by parabolic well $\mathcal{V} = K(R_x^2 + R_y^2)/2$, the real-time dynamics of the skyrmion is oscillatory with two characteristic circular modes given by

$$\tilde{\omega}_\pm = -\frac{\tilde{Q}}{2\mathcal{M}} \pm \sqrt{\left(\frac{\tilde{Q}}{2\mathcal{M}}\right)^2 + \frac{K}{\mathcal{M}}}, \quad (34)$$

where we have introduced $\mathcal{M} = \mathcal{M}_{xx} = \mathcal{M}_{yy}$. Finally, the most general case of an anisotropic potential \mathcal{V} gives rise to four distinct circular modes, originating from the fact that the mass tensor elements are no longer equal, a result that could possibly have interesting experimental implications.

IV. CHIRAL MAGNETS

In this section, we apply the formalism derived in the previous section explicitly to a skyrmionic magnetic texture, focusing on the low temperature contribution to the mass, in the presence of a perturbation in the free energy that breaks translational symmetry. Skyrmions, known to be stable or metastable solutions in chiral magnets with an applied magnetic field, are described on a square lattice by the spin Hamil-

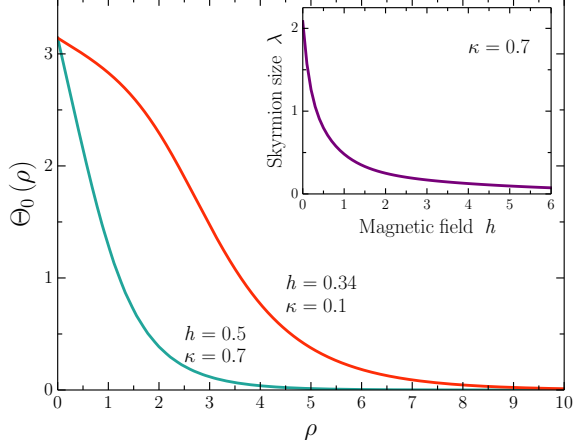


FIG. 2. (color online). Magnetization profiles $\Theta_0(\rho)$ of a skyrmion as function of radial distance ρ for a small radius skyrmion with chosen easy-axis anisotropy $\kappa = 0.7$ and magnetic field $h = 0.5$ (green line) and a large-radius skyrmion with $\kappa = 0.1$ and $h = 0.34$ (red line). Magnetic field is applied along the easy-axis (all parameters given in scaled dimensionless units, see text). The inset depicts the dependence of the skyrmion radius λ on h for $\kappa = 0.7$.

tonian,

$$H_s = -\tilde{J} \sum_{a,i} \mathbf{S}_a \cdot \mathbf{S}_{a+e_i} - \tilde{K} \sum_a (S_a^z)^2 - g\mu_B \tilde{H} \sum_a S_a^z - \tilde{D} \sum_a [(\mathbf{S}_a \times \mathbf{S}_{a+e_x}) \cdot \hat{x} + (\mathbf{S}_a \times \mathbf{S}_{a+e_y}) \cdot \hat{y}]. \quad (35)$$

Here, $\mathbf{S}_a = (S_a^x, S_a^y, S_a^z)$ is the spin of size S at lattice site a and $\mathbf{e} = (e_x, e_y)$ is the lattice unit vector. We assume the on-site anisotropy constant to be positive, $\tilde{K} > 0$, so that there is an easy axis along z and fix the chirality of the Dzyaloshinskii-Moriya (DM) interaction, \tilde{D} . The strength of the magnetic field along the z axis is \tilde{H} and the exchange interaction constant is assumed to be ferromagnetic, $\tilde{J} > 0$.

Using coherent state representation for the spins (assuming $S \gg 1$) and passing to the continuum limit³¹, we find that Eq. (35) corresponds to the free energy of the form

$$\mathcal{F}(\mathbf{m}) = J \sum_{i=x,y} \left(\frac{\partial \mathbf{m}}{\partial \tilde{r}_i} \right)^2 + D \mathbf{m} \cdot \nabla \times \mathbf{m} - K m_z^2 - H m_z, \quad (36)$$

where $J = \tilde{J}S^2$, $K = \tilde{K}S^2/\alpha^2$, $H = g\mu_B \tilde{H}S^2/\alpha^2$, and $D = \tilde{D}S^2/\alpha$. We now introduce dimensionless spatial variables $\mathbf{r} = \tilde{\mathbf{r}}/(l\alpha)$ where $l = \tilde{J}/\tilde{D} = J/(D\alpha)$, while energies are measured in units of $\varepsilon_\Lambda = \tilde{J}S^2 = J$. The energy density in reduced units is defined as $w(\Phi, \Pi) = \frac{(l\alpha)^2}{\varepsilon_\Lambda} \mathcal{F}(\Phi, \Pi)$ (see Eq. (A1)). We consider the regime of isolated skyrmions, which exist for a wide range of parameters K and H as a stable or metastable state. A skyrmion with $Q = -1$ is

parametrized by (see Appendix A)

$$\Theta_0(\mathbf{r}) = \Theta_0(\rho), \quad \Phi_0(\mathbf{r}) = \phi \pm \pi/2, \quad (37)$$

while the helicity, defined by the sign in Φ_0 , is commensurate with the DM interaction. The structure of the stationary skyrmion $\Theta_0(\rho)$ is determined by the Euler-Lagrange equation derived from skyrmion energy $w(\Phi_0, \Pi_0)$ and is given in Eq. (A4). Because there is no known analytic solution for $\Theta_0(\rho)$, the following function can be used as an approximate solution,

$$\Theta_0(\rho) = 2 \tan^{-1} \left(\frac{\lambda}{\rho} e^{-\frac{\rho-\lambda}{\rho_0}} \right). \quad (38)$$

Roughly speaking, $\rho_0 = \sqrt{2/(2\kappa + h)}$ determines the amount of spins that are *non-collinear* with the easy axis, while λ , which we obtain numerically using an algorithm based on Runge-Kutta formulas⁴⁰, is the skyrmion radius of the area for which the spins are *parallel* to the easy axis. Here, $\kappa = \tilde{K}\tilde{J}/\tilde{D}^2$ and $h = g\mu_B \tilde{H}\tilde{J}/\tilde{D}^2$ are the dimensionless parameters describing easy-axis anisotropy and magnetic field, respectively (see Table. I). In the opposite limit of a large-radius skyrmion the magnetization profile is described by

$$\cos \Theta_0(\rho) = \tanh\left(\frac{\rho - \lambda}{\Delta_0}\right), \quad (39)$$

where the parameters λ and Δ_0 are calculated numerically by fitting the approximate function (39) to the numerical solution of the Euler-Lagrange equation (A4). Magnetization profiles of skyrmions in the small and large radius limit obtained numerically are depicted in Fig. 2. A detailed discussion of the magnon eigenstates Ψ_n is provided in Appendix B. Apart from the magnon scattering states Ψ_n^{sc} that lie above the magnon gap $\varepsilon_{\text{MS}} = \kappa + h/2$, induced by the anisotropy and magnetic field, there exist massive internal modes Ψ_n^{bs} that are found for energies $0 < \varepsilon_n \leq \varepsilon_{\text{MS}}$. These bound states correspond to deformations of the skyrmion into breathing modes and were discovered numerically in Refs. 37 and 41.

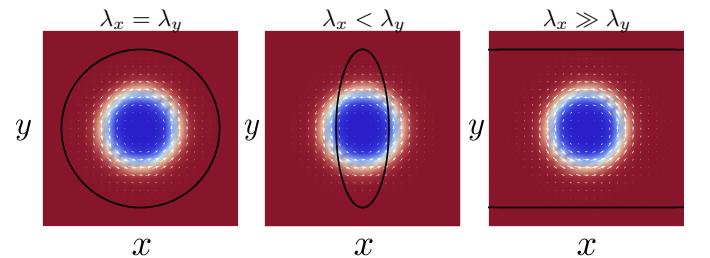


FIG. 3. (color online). Pictorial representation of a skyrmion in the presence of a magnetic trap described by Eq. (40) for different magnetic trap sizes. The coloured surface represents the out of plane component of the magnetization texture of a skyrmion with positive maximum at the center (blue), while black solid line represents the size of the trap.

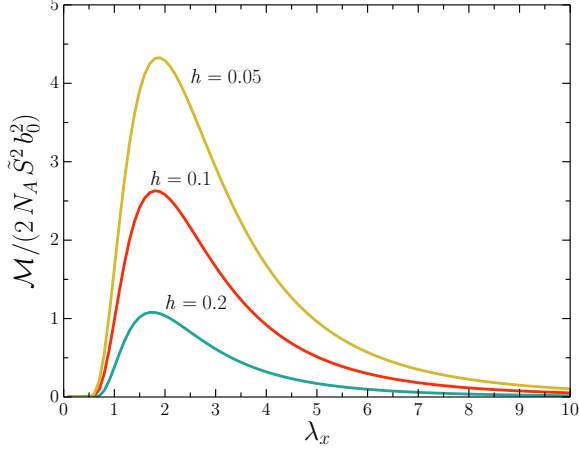


FIG. 4. (color online). Dependence of the mass term \mathcal{M} on the trap size $\lambda_x = \lambda_y$ of an isotropic magnetic trap of strength $b_0 = 0.1$ at $T = 0$. The skyrmion configuration is described by the parameters $\kappa = 0.7$, and three values of magnetic field $h = 0.2, 0.1, 0.05$ with skyrmion radius $\lambda = 1.26, 1.57, 1.79$, respectively.

V. SKYRMION MASS AT ZERO TEMPERATURE

The mass tensor \mathcal{M}_{ij} of a magnetic skyrmion in the zero temperature limit is now investigated. From Eq. (33) it becomes apparent that in the $\beta \rightarrow \infty$ limit only the mass term \mathcal{M}_{ij}^0 survives, which is in turn non zero only in the presence of a perturbation in the free energy that breaks translational symmetry. We consider three isotropic mechanisms for the generation of a skyrmion mass, all breaking translational invariance. (1) a magnetic trap, generated by a non-uniform magnetic field, (2) a local defect that alters the exchange constant, and (3) a periodic variation in the exchange constant. In all three cases, we assume the translationally non-invariant terms to be much smaller than those that are translationally symmetric, $|\int d\mathbf{r} \mathcal{V}(\Phi_0, \Pi_0)| \ll S_E$, and they can thus be treated perturbatively. In all cases where an isotropic potential in x and y direction is applied, we find $\mathcal{M}_{xx}^0 = \mathcal{M}_{yy}^0 = \mathcal{M}$, whereas $\mathcal{M}_{xy} = -\mathcal{M}_{yx}$ and thus, being antisymmetric, they do not contribute to the equation of motion, Eq. (27).

A simple realization of a magnetic trap is

$$\mathbf{b}(\mathbf{r}) = -b_0 e^{-\frac{x^2}{\lambda_x^2} - \frac{y^2}{\lambda_y^2}} \hat{z}, \quad (40)$$

where λ_x and λ_y characterize the size of the trap along the x and y directions, respectively. See Fig. 3 for a visualization of the radially symmetric, $\lambda_x = \lambda_y$, and asymmetric, $\lambda_x \neq \lambda_y$, magnetic traps. Because the propagating magnon modes are suppressed, we numerically calculate the mass terms by including only the lowest energy bound states, which are themselves found variationally, in the sum of Eq. (31). In Fig. 4 we plot these results as a function of λ_x for a radially symmetric trap, $\lambda_y = \lambda_x$, where we have a chosen $\kappa = 0.7$, $b_0 = 0.1$ and three values of magnetic field $h = 0.2, 0.1, 0.05$ with skyrmion radius $\lambda = 1.26, 1.57, 1.79$ respectively. For λ_x

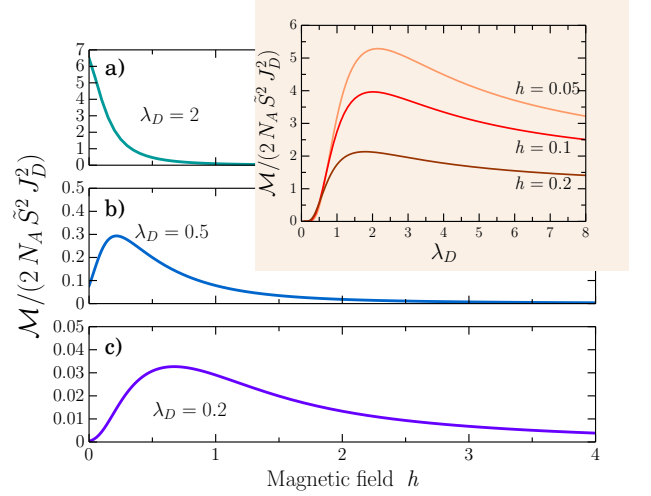


FIG. 5. (color online). Magnetic field dependence of the mass term \mathcal{M} in the presence of a defect for a skyrmion with $\kappa = 0.7$, $J_D = 0.1$ at $T = 0$. We depict three different values of defect size $\lambda_D = 2, 0.5, 0.2$. The inset shows the dependence of \mathcal{M} on the defect size λ_D for a skyrmion with $h = 0.2, 0.1, 0.05$ and skyrmion radius $\lambda = 1.26, 1.57, 1.79$, respectively.

smaller than a critical value $\lambda_x^{cr} \sim \lambda$, the mass increases with increasing λ_x , while for $\lambda_x \gtrsim \lambda_x^{cr}$ the mass decreases monotonically.

When there is a local defect in the crystal structure of the chiral magnet, e.g. at the origin, the exchange interaction is a function of position around that point which we model as

$$J \rightarrow J_0 - J_D e^{-\rho/\lambda_D}, \quad (41)$$

where J_D and λ_D parameterize the strength and size of the defect, respectively.

In Fig. 5 we plot the skyrmion mass due to such a defect as a function of applied magnetic field for several values of λ_D and $J_D = 0.1$. The behavior of Fig. 5 implies that as long as $\lambda_D < \lambda$, the mass \mathcal{M} increases with increasing/decreasing magnetic field/skyrmion size, peaking around $\lambda_D \sim \lambda$ and then for $\lambda_D > \lambda$ decreases with decreasing skyrmion size (see Fig. 5(b) and (c)). We see no peak when $\lambda_D = 2$, Fig. 5(a), because the skyrmion radius for all positive magnetic fields is smaller than the size of the defect. In addition, the dependence of \mathcal{M} on λ_D is presented in the inset of Fig. 5, where a peaked behaviour is suggested with a maximum around λ . We note that although it has been shown that a model with spatially dependent exchange interactions similar to Eq. (41) act as a pinning potential⁴², i.e., $\partial\mathcal{V}/\partial\mathbf{R}_i$ in Eq. 27, our findings show that additionally a finite mass is generated. Finally, because of the discrete underlying lattice the exchange interaction can obtain a periodic modulation along the lattice vectors,

$$J \rightarrow J_0 - J_P \cos(x/\lambda_P) - J_P \cos(y/\lambda_P), \quad (42)$$

where J_P and λ_P are the strength and period, respectively, by which the exchange deviates from J_0 . In Fig. 6 we plot the magnetic field dependence of \mathcal{M} for $\lambda_P = 1.5$ and $J_P = 0.1$. Focusing on the dependence of \mathcal{M} on the skyrmion radius

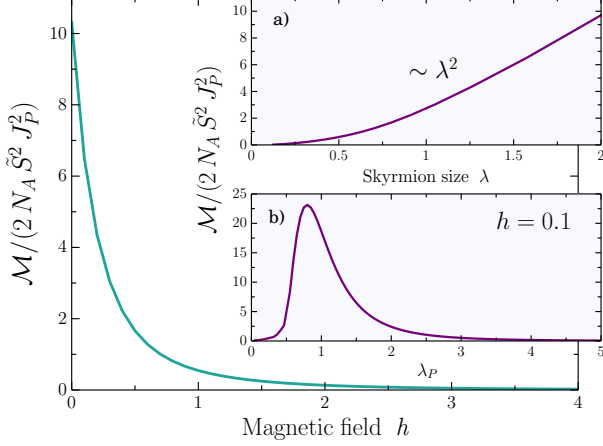


FIG. 6. (color online). Magnetic field dependence of the mass term \mathcal{M} for spatially dependent periodic exchange interactions with $\lambda_P = 1.5$, $J_P = 0.1$ and $T = 0$. Inset a) depicts the λ^2 dependence of \mathcal{M} , while inset b) illustrates \mathcal{M} as a function of period λ_P for $h = 0.1$.

λ , illustrated in the inset of Fig. 6 (a), it becomes apparent that \mathcal{M} grows with the area λ^2 . Further results are provided in inset Fig. 6 (b), where we examine the dependence of the mass on the period λ_P for $h = 0.1$, $\lambda = 1.57$, and $J_P = 0.01$. Fig. 6 (b) reveals a peaked behaviour around $\lambda/2$.

A. Massive Skyrmion in 1D

The case of a magnetic skyrmion confined in a quasi-one dimensional space can be realized by applying an anisotropic magnetic trap whose size is much larger in one spatial direction than in the other, *i.e.*, $\lambda_x \gg \lambda_y$. A pictorial representation of a skyrmion in the presence of an anisotropic magnetic trap is provided in Fig. 3. When $\lambda_x \neq \lambda_y$, the elements of the mass tensor \mathcal{M}_{ij}^0 are no longer equal, but acquire different values depending on the size of the magnetic trap. In Fig. 7 we plot the dependence of \mathcal{M}_{xx}^0 and \mathcal{M}_{yy}^0 on λ_x for a fixed value of $\lambda_y = 2$ and a skyrmion with $\kappa = 0.7$, $h = 0.1$ and $\lambda = 1.57$. We find that \mathcal{M}_{xx}^0 is maximized at λ ; conversely, \mathcal{M}_{yy}^0 grows until $\lambda_y \sim \lambda_x$ upon which it approaches a constant value.

A corollary of the preceding discussion is that the highly anisotropic magnetic trap acts as a *magnetic quantum wire*, along which the skyrmion moves as a massive particle due to its one-dimensional confinement. Our investigation demonstrates that skyrmions observed in confined geometries such as magnetic nanowires⁴⁴ exhibit fundamentally different dynamical behaviour compared to the one in unconfined 2D geometries. It would be interesting to test this prediction.

VI. SKYRMION MASS AT FINITE TEMPERATURE

When no translational symmetry breaking term is present, the only contribution to the mass is given by the term \mathcal{M}_{ij}^T ,

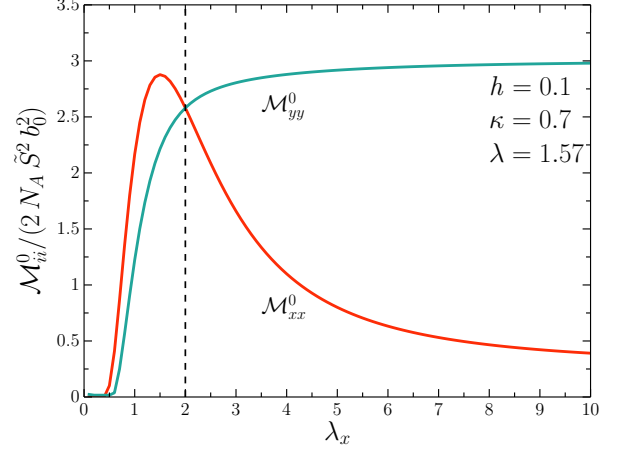


FIG. 7. (color online). Dependence of the mass terms \mathcal{M}_{xx}^0 , \mathcal{M}_{yy}^0 and off-diagonal elements $\mathcal{M}_{xy} = iM_{yx}$ on the trap size λ_x of an anisotropic magnetic trap of strength $b_0 = 0.1$ and fixed $\lambda_y = 2$. The skyrmion configuration is described by the parameters $\kappa = 0.7$, $h = 0.1$, and $\lambda = 1.57$. The dashed vertical line indicates the location of $\lambda_y = 2$.

which is non-vanishing for finite temperatures in general. The series expression Eq. (33) requires the summation over the full magnon spectrum, that is over scattering states $\Psi_{m,k}^{\text{sc}}$ which are classified by the azimuthal quantum number m as well as the radial momentum $k \geq 0$ with energy $\varepsilon_k = \varepsilon_{\text{MS}} + k^2$, with $\varepsilon_{\text{MS}} = \kappa + h/2$. In addition to scattering states, one needs to take into account localized modes Ψ_m^{bs} , classified by m with energies in the range $0 < \varepsilon_m \leq \varepsilon_{\text{MS}}$. Therefore we consider the following terms,

$$\mathcal{M}_{ij}^T = \mathcal{M}_{ij}^{\text{sc}} + \mathcal{M}_{ij}^{\text{bs}} + \mathcal{M}_{ij}^{\text{bs-sc}}, \quad (43)$$

where $\mathcal{M}_{ij}^{\text{sc}}$ denotes the contribution from scattering states, $\mathcal{M}_{ij}^{\text{bs}}$ the contribution from bound states, and $\mathcal{M}_{ij}^{\text{bs-sc}}$ takes into account combinations of bound–scattering states. Here, we focus on large-radius skyrmions for low magnetic fields and easy-axis anisotropy, where the skyrmion is expected to support more internal modes with energy below ε_{MS} than for small radius-skyrmions. As the magnetic field or easy axis anisotropy are increased, the radius decreases and the modes sequentially leave the gap region, pass to the continuous spectrum and transform into quasi-localized modes. Therefore, there is a bounded parameter region of h and κ where the requirement $\varepsilon_m \leq \varepsilon_{\text{MS}}$ is fulfilled.

A calculation of bound and scattering states is presented in Appendix B, while explicit expressions for $\mathcal{M}_{ij}^{\text{sc}}$, $\mathcal{M}_{ij}^{\text{bs}}$, and $\mathcal{M}_{ij}^{\text{bs-sc}}$ are given in Appendix C. From the form of the matrix elements $\mathcal{B}_{ij}^{n,n'}$ of Eq. (23) we conclude that only combinations of states with angular momentum difference $\Delta m = \pm 1$ contribute to the finite T skyrmion mass \mathcal{M}_{ij}^T . From the variational calculation of bound state energies in the large skyrmion limit for the parameter range considered here, we find two localized modes below the magnon continuum with $m = 0$ and $m = 2$. Therefore, we find vanishing contributions from the

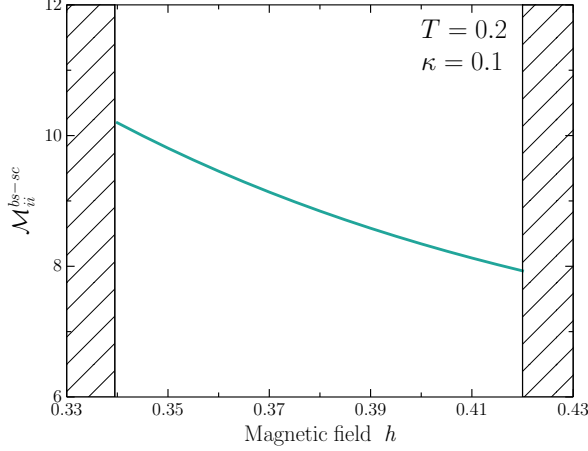


FIG. 8. (color online). Magnetic field dependence of diagonal mass tensor elements \mathcal{M}_{ii}^{bs-sc} for a skyrmion with $\kappa = 0.1$, at temperature $T = 0.2$ and for $S = 1$ and $\tilde{J}/\tilde{D} = 4$. The magnetic field region where bound states contribute to the mass is bounded by the critical field below which the skyrmion becomes unstable (left vertical line) up to the field where the bound state energy passes to the continuous spectrum (right vertical line).

term \mathcal{M}_{ij}^{bs} because the zero mode with $m = 1$ is excluded from the summations. The behaviour of \mathcal{M}_{ij}^{bs-sc} for a skyrmion with $\kappa = 0.1$, $S = 1$ and $\tilde{J}/\tilde{D} = 4$ as a function of h for $T = 0.2$ is summarized in Fig. 8, while the main features of \mathcal{M}_{xx}^{sc} as a function of T and h are depicted in Fig. 9. Summations over the quantum number m converge rapidly and are bounded between $-7 \leq m \leq 7$. In Fig. 9, we calculate \mathcal{M}_{ij}^T for a discrete set of h and T and then we adopt a smoothing process to obtain the mass that is a reasonably smoothed function of (h, T) .

VII. DISCUSSION

Skyrmion phases have been observed in several metallic ferromagnets, including MnSi³ and FeGe⁴⁵, as well as in the insulator Cu₂OSeO₃^{46,47}. Typical parameter values for Cu₂OSeO₃ crystals are $\tilde{J} = 33.36 \cdot 10^{-4}$ eV, $\tilde{D} = 7.47 \cdot 10^{-4}$ eV and $\alpha = 8.911$ Å ($\tilde{J}/\tilde{D} = 4.46$)⁴⁸. For these values, the mass is measured in units of approximately $N_A \cdot 4.1 \cdot 10^{-26}$ kg, which corresponds to about $4.5 \cdot 10^4$ electron masses.

Equation (31) is the first closed formula for the mass of a skyrmion, obtained microscopically in the presence of arbitrary external perturbations arising from defects, non-uniform magnetic fields, and external potentials and at arbitrary temperature. The problem of the inertia properties of skyrmions has been addressed in Ref. [18] by means of numerical solutions of the classical stochastic LLG equation in the presence of random thermal forces and a time-dependent magnetic field gradient. Among the results so obtained is a large numerical value of the effective mass as well as a peculiar type of damping that enters as $\mathbf{\Gamma} \times \dot{\mathbf{R}}$ in Newton's equation, with

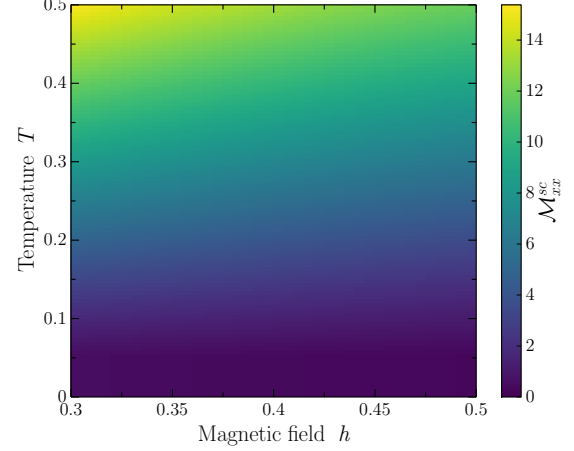


FIG. 9. (color online). The colored surface represents the mass term \mathcal{M}_{xx}^{sc} calculated for a skyrmion with $\kappa = 0.1$, $S = 1$, and $\tilde{J}/\tilde{D} = 4$ as a function of magnetic field h and temperature T .

$\mathbf{\Gamma} \parallel \hat{z}$. It was reported that both the mass and $\mathbf{\Gamma}$ are proportional to the area of the skyrmion, a result that is consistent with our theoretical finding depicted in Fig. 6. In Ref.[49] an inertia term was estimated that appears due to a confining potential, independent of the skyrmion size λ and proportional to the stiffness of the harmonic confining potential. Finally, it is also worth mentioning that an approximate evaluation of the mass term of a skyrmion magnetic bubble, a circular domain wall stabilized by long range interactions has been found in Ref.[19], derived by generalizing Thiele's approach beyond steady motion. We emphasize that the mass tensor depends on the inverse of the magnon energy ε_n . We therefore expect that bound states, which correspond to deformations of the skyrmion with energies below the gap, have a larger contribution. This finding is consistent with Ref. [19] where an approximate value for the mass of a magnetic bubble domain has been calculated by considering contributions from distortions of the circular domain wall. In addition, a large value of inertial mass of a magnetic bubble has been experimentally reported in Ref. [39]. The bubbles were subjected to a local parabolic magnetic potential which originates from irregularities of the magnetic film and the presence of an inertial mass was attributed to a breathing mode associated with a change of the bubble size. While several studies demonstrate the association of inertia mass to deformations of the skyrmion, an explicit analytical formula was missing so far and has been provided here. Our detailed calculations shed light on the mechanism of mass generation, and we also provide an analytic formula, valid in the presence of arbitrary external perturbations which can serve as a basis for a variety of further studies.

VIII. CONCLUDING REMARKS

The main task of the paper is to describe dissipation of a magnetic skyrmion using the canonical scheme of quantization. Within this formalism the skyrmion position is promoted to a time-dependent dynamical variable and a finite perturbation theory in terms of fluctuations around the skyrmionic configuration is performed. The interaction of the skyrmion with these magnon modes gives rise to a damping term that is found to be time-dependent, in contrast to the typical Gilbert damping. The time-dependence of damping kernel indicates that damping depends on the velocity of the skyrmion of the past.

Perhaps, the most interesting feature is that the effect of damping is reduced to a mass term in some limits. We demonstrate that a massless skyrmion at the classical level is a consequence of the translational symmetry assumed for the system. Our investigation suggests that, at zero temperature, the skyrmion mass is non-zero in the presence of an external perturbation arising from defects, non-uniform magnetic fields and external potentials. Among the translational symmetry breaking terms we have considered here, we emphasize the case of a quasi-one dimensional wire provided by an anisotropic magnetic trap, along which the skyrmion moves as a massive particle owing to its confinement.

To complete the description we have also examined damping at finite temperatures where we find that it is present even in the absence of perturbations. This picture suggests that in the absence of perturbations, massive magnon modes are activated at finite temperatures. A utilization of the improved skyrmion dynamics calculated in the present paper could be towards the direction of investigating the possibility of de-

pinning via quantum tunneling, a behavior that has been studied both theoretically⁵⁶ and experimentally⁵⁷ in similar mesoscopic magnetic structures, such as magnetic domain walls.

In our present study, we have exclusively focused on damping caused by intrinsic mechanisms originating from the interaction of the skyrmion with magnon modes which it generates and couples back to, giving rise to damping. Additional sources of damping could arise if one takes into account time-dependent forces or the interaction of the skyrmion to extrinsic degrees of freedom, like a current of electrons or phonons. However, this is beyond the scope of this work, and we leave it as a motivation for further studies making use of the general formalism developed here.

ACKNOWLEDGEMENTS

We would like to acknowledge Peter Stano and Achim Rosch for useful discussions. This work was supported by the Swiss National Science Foundation (SNSF) and NCCR QSIT.

Appendix A: Skyrmion as Saddle Point Configuration

In this Appendix we give the explicit form of the skyrmion by finding the approximate saddle point configuration of the free energy of Eq. (36). It is convenient to introduce dimensionless spatial variables $\mathbf{r} = \tilde{\mathbf{r}}/(l\alpha)$, where $l = \tilde{J}/\tilde{D} = J/(D\alpha)$, and $\varepsilon_\Lambda = J = \tilde{J}S^2$ is a characteristic energy scale. The energy density of the spin configuration in reduced units $w(\Phi, \Pi) = \frac{(l\alpha)^2}{\varepsilon_\Lambda} \mathcal{F}(\Phi, \Pi)$ in polar coordinates $\mathbf{r} = (\rho \cos \phi, \rho \sin \phi)$ is given by

$$w(\Phi, \Pi) = (\nabla\Theta)^2 + \sin^2\Theta(\nabla\Phi)^2 - \kappa \cos^2\Theta - h \cos\Theta + \left(\cos(\phi - \Phi) \frac{\partial\Theta}{\partial\rho} - \sin\Theta \cos\Theta \sin(\phi - \Phi) \frac{\partial\Phi}{\partial\rho} - \frac{1}{\rho} \sin(\phi - \Phi) \frac{\partial\Theta}{\partial\phi} - \frac{1}{\rho} \sin\Theta \cos\Theta \cos(\phi - \Phi) \frac{\partial\Phi}{\partial\phi} \right), \quad (\text{A1})$$

where $\kappa = KJ/D^2$ and $h = HJ/D^2$. The functional (A1) produces a rich phase diagram of magnetic phases, including a cone phase, a helicoid phase, isolated skyrmions, and skyrmion lattices^{50–52}. In the presence of additional interactions, such as Rashba spin-orbit coupling, the stability of skyrmion phases is enhanced over a large range of magnetic fields⁵³. In the following we will consider the regime of isolated skyrmions which exists for a wide range of parameters κ and h as a metastable state of the ferromagnetic background $\mathbf{m} = (0, 0, 1)$. Rotationally symmetric solutions are described by

$$\Theta_0(\rho, \phi) = \Theta_0(\rho), \quad \Phi_0(\rho, \phi) = \phi + \pi/2, \quad (\text{A2})$$

for a skyrmion with topological number $Q = -1$. The skyrmion energy with respect to the uniform state is,

$$w_0(\Phi_0, \Pi_0) = (\nabla\Theta_0)^2 + \left(\frac{1}{\rho^2} + \kappa \right) \sin^2\Theta_0 + h(1 - \cos\Theta_0) + \Theta'_0 + \frac{1}{\rho} \sin\Theta_0 \cos\Theta_0. \quad (\text{A3})$$

The structure of the stationary skyrmion is determined by the Euler-Lagrange equation,

$$\Theta''_0(\rho) + \frac{\Theta'_0(\rho)}{\rho} - \frac{\sin\Theta_0 \cos\Theta_0}{\rho^2} + \frac{\sin^2\Theta_0}{\rho} - \frac{h}{2} \sin\Theta_0 - \frac{\kappa}{2} \sin 2\Theta_0 = 0, \quad (\text{A4})$$

with boundary conditions $\Theta_0(0) = \pi$ and $\Theta_0(\infty) = 0$. Because there is no known analytic solution, the following func-

tion can be used as an approximate solution

$$\Theta_0(\rho) = 2 \tan^{-1} \left(\frac{\lambda}{\rho} e^{-\frac{\rho-\lambda}{\rho_0}} \right), \quad (\text{A5})$$

where $\rho_0 = \sqrt{2/(2\kappa + h)}$. The skyrmion radius λ can be determined by fitting the Ansatz (A5) to the one obtained numerically using an algorithm based on Runge–Kutta formulas⁴⁰. In the opposite limit of a large-radius skyrmion the magnetization profile is described by

$$\cos \Theta_0(\rho) = \tanh\left(\frac{\rho - \lambda}{\Delta_0}\right), \quad (\text{A6})$$

where the parameters λ and Δ_0 are again calculated numerically by fitting the approximate function (A6) to the numerical solution of the Euler-Lagrange equation (A4). Magnetization profiles of skyrmions in the small-radius limit are depicted in Fig. 2.

Appendix B: Magnon Spectrum

Here we consider the spectrum of the magnon modes on the skyrmion background. Magnon scattering states are obtained for energies $\varepsilon_n \geq \varepsilon_{\text{MS}}$, with $\varepsilon_{\text{MS}} = \kappa + h/2$. In addition to scattering states, we expect localized modes that correspond to deformations of the skyrmion into polygons (breathing modes) in the range $0 < \varepsilon_n < \varepsilon_{\text{MS}}$. The existence of such modes was found numerically in Refs. [41] and [37]. An extensive analysis of the magnon spectrum has been provided in Ref. [37], where the authors numerically determine the magnon bound states and provide an analytical and numerical description of magnon scattering states. Here we repeat some steps of the analysis adapted to our purpose and introduce a variational approach for the calculation of the bound states in the small and large radius limit of skyrmions.

To begin with, we seek for solutions of the eigenvalue problem (EVP) $\mathcal{H}\Psi_n = 2\sigma_z \varepsilon_n \Psi_n$, where the Hamiltonian is given by

$$\mathcal{H} = 2[-\nabla^2 + U_0(\rho)]\mathbb{1} + 2W(\rho)\sigma_x - 2iV(\rho)\frac{\partial}{\partial\phi}\sigma_z. \quad (\text{B1})$$

Here, the potential terms $V(\rho)$, $W(\rho)$, and $U_0(\rho)$ are defined by

$$\begin{aligned} V(\rho) &= \frac{2 \cos \Theta_0}{\rho^2} - \frac{\sin \Theta_0}{\rho}, \\ W(\rho) &= \frac{\sin 2\Theta_0}{4\rho} - \frac{(\Theta'_0)^2}{2} + \frac{1}{2}\left(\kappa + \frac{1}{\rho^2}\right) \sin^2 \Theta_0 - \frac{\Theta'_0}{2}, \end{aligned} \quad (\text{B2})$$

and

$$\begin{aligned} U_0(\rho) &= \frac{h \cos \Theta_0}{2} - \frac{3 \sin 2\Theta_0}{4\rho} - \frac{(\Theta'_0)^2}{2} \\ &\quad + \left(\frac{\kappa}{4} + \frac{1}{4\rho^2}\right)(1 + 3 \cos 2\Theta_0) - \frac{\Theta'_0}{2}, \end{aligned} \quad (\text{B3})$$

where the quantum number n labels both localized modes and scattering states. Next, we represent solutions in terms of wave expansions $\Psi_n = e^{im\phi}\psi_{n,m}(\rho)$, and the EVP is written as $\mathcal{H}_m\psi_{n,m}(\rho) = \varepsilon_{n,m}\sigma_z\psi_{n,m}(\rho)$ with

$$\mathcal{H}_m = (-\nabla_\rho^2 + U_0(\rho) + \frac{m^2}{\rho^2})\mathbb{1} + V(\rho)m\sigma_z + W(\rho)\sigma_x, \quad (\text{B4})$$

where $\nabla_\rho^2 = \frac{\partial^2}{\partial\rho^2} + \frac{1}{\rho}\frac{\partial}{\partial\rho}$ is the radial Laplace operator. These eigenfunctions are normalized such that

$$\int_0^\infty d\rho \rho \psi_{n,m}^\dagger(\rho) \sigma_z \psi_{n',m}(\rho) = \delta_{n,n'}. \quad (\text{B5})$$

In Ref. [37] it was stated that apart from the class of solutions $\Psi_{n,m} = e^{im\phi}\psi_{n,m}$ with energy $\varepsilon_{n,m}$, there exist solutions $\Phi_{n,-m} = K\sigma_x\Psi_{n,m} = e^{-im\phi}\sigma_x\psi_{n,m} = e^{-im\phi}\phi_{n,-m}$ with energy $-\varepsilon_{n,m}$. Here K is the operator of complex conjugation. Since magnons can not be described by negative-energy quantum states, we focus on positive energies $\varepsilon_{n,m} > 0$ and use the $\sigma_x K$ transformation only in the $\varepsilon_{n,m} = 0$ case. For example, if

$$\Psi_1 = e^{i\phi} \frac{1}{\sqrt{8}} \begin{pmatrix} \Theta'_0 - \frac{1}{\rho} \sin \Theta_0 \\ \Theta'_0 + \frac{1}{\rho} \sin \Theta_0 \end{pmatrix} \quad (\text{B6})$$

is one translational mode with zero energy, then we recover the second mode as,

$$\Phi_{-1} = K\sigma_x\Psi_1 = e^{-i\phi} \frac{1}{\sqrt{8}} \begin{pmatrix} \Theta'_0 + \frac{1}{\rho} \sin \Theta_0 \\ \Theta'_0 - \frac{1}{\rho} \sin \Theta_0 \end{pmatrix}. \quad (\text{B7})$$

1. Small-Radius Skyrmion

For magnetic solitons in 2D easy-axis ferromagnets in the small-radius limit there is a bound state with $m = -1$ that remains localized and is associated with the soliton displacement⁵⁴. We extend these results to the skyrmion field,

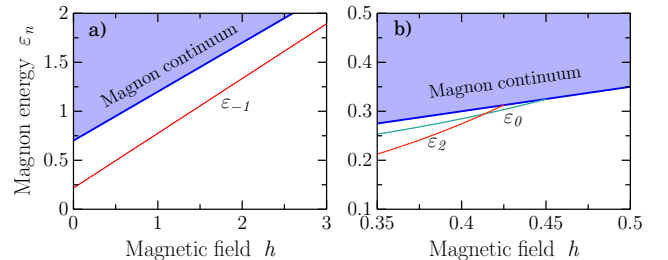


FIG. 10. (color online). Magnetic field dependence of the energy of the localized mode with (a) $m = -1$ for a skyrmion with $\kappa = 0.7$ described by Eq. (B8) and (b) with $m = 0$ and $m = 2$ for a skyrmion with $\kappa = 0.1$ described by Eq. (B10). Shaded areas depict the magnon continuum with boundary line ε_{MS} .

and we seek for a localized mode with $m = -1$ by performing a variational calculation. We choose trial functions $\Psi_{-1} = e^{-i\phi}\psi_{-1}(\rho)$ as⁵⁴

$$\psi_{-1}(\rho) = \begin{pmatrix} \Theta'_0 - \sin \Theta_0/\rho + a\rho^2\Theta'_0 - b\rho \sin \Theta_0 \\ \Theta'_0 - \sin \Theta_0/\rho + a\rho^2\Theta'_0 + b\rho \sin \Theta_0 \end{pmatrix}, \quad (\text{B8})$$

and minimize the functional

$$\mathcal{U} = \int d\rho \rho \psi_{-1}^\dagger(\rho)(\mathcal{H}_{-1} - \varepsilon_{-1}\sigma_z)\psi_{-1}(\rho) \quad (\text{B9})$$

with respect to the variational parameters a and b in order to calculate the energy ε_{-1} . Then, the parameters a and b can be found from the normalization conditions (B5). In Fig. 10 (a) we illustrate the energy ε_{-1} as a function of magnetic field h for $\kappa = 0.7$. Within the limits of the variational approach, we find $\varepsilon_{-1} < \varepsilon_{\text{MS}}$ for a wide range of magnetic fields up to $h = 8$.

2. Large-Radius Skyrmion

In the limit of large radius, the magnetization profile of the skyrmion is described by Eq. (A6) and the localized modes Ψ_m^{bs} with energy ε_m are again found variationally, but now using the trial functions⁴³

$$\Psi_m^{\text{bs}}(\mathbf{r}) = \frac{1}{\sqrt{2\pi}} e^{im\phi} \begin{pmatrix} a_m f_0(\rho) \\ b_m f_0(\rho) \end{pmatrix}, \quad (\text{B10})$$

where $f_0(\rho) = A/\cosh(\frac{\rho-\lambda}{\Delta_0})$ and A is chosen such that $\int d\rho \rho f_0^2 = 1$. The condition of minimizing the energy functional $\mathcal{U} = \int d\mathbf{r} (\Psi_m^{\text{bs}})^\dagger (\mathcal{H}_m - \sigma_z \varepsilon_m) \Psi_m^{\text{bs}}$, along with normalization conditions satisfied by the functions $\Psi_m^{\text{bs}}(\rho)$ will specify the eigenenergies ε_m as well as the variational parameters a_m and b_m . In Fig. 10 (b) we display the energies ε_0 and ε_2 as a function of magnetic field h for $\kappa = 0.1$.

3. Scattering States

To complete the description of the magnon spectrum we need to include the scattering states $\Psi_{m,k}^{\text{sc}}(\mathbf{r})$ classified by m as well as the radial momentum $k \geq 0$. Here we repeat some steps of the calculation of $\Psi_{m,k}^{\text{sc}}(\mathbf{r})$ originally presented in Ref. [37] for reasons of a complete discussion. In the absence of a skyrmion, magnon scattering states are described by

$$\mathcal{H}_m^0 = (-\nabla_\rho^2 + \frac{m^2 + 1}{\rho^2} + \varepsilon_{\text{MS}})\mathbb{1} + \frac{2m}{\rho^2}\sigma_z, \quad (\text{B11})$$

and the eigenvalue problem $\mathcal{H}_m^0 \psi_{m,k}^{\text{free}} = \varepsilon_k \psi_{m,k}^{\text{free}}$ is solved by

$$\psi_{m,k}^{\text{free}} = \nu_m J_{m+1}(k\rho) \begin{pmatrix} 1 \\ 0 \end{pmatrix}, \quad (\text{B12})$$

where J_m are the Bessel functions of the first type, ν_m a normalization constant and $\varepsilon_k = \varepsilon_{\text{MS}} + k^2$, with $\varepsilon_{\text{MS}} = \kappa + h/2$. In

the presence of a skyrmion the scattering problem of Eq. (B4) is reformulated as $\mathcal{H}_m = \mathcal{H}_m^0 + \mathcal{V}_m^{\text{sc}}$ with

$$\mathcal{V}_m^{\text{sc}} = u_0(\rho)\mathbb{1} + \left[V(\rho) - \frac{2}{\rho^2} \right] m\sigma_z + W(\rho)\sigma_x, \quad (\text{B13})$$

with potential $u_0(\rho) = U_0(\rho) - \frac{h}{2} - \frac{1}{\rho^2} - \kappa$. In this case, the solutions of the eigenvalue problem $\mathcal{H}_m \psi_{m,k}^{\text{sc}} = \varepsilon_k \psi_{m,k}^{\text{sc}}$ are

$$\psi_{m,k}^{\text{sc}}(\rho) = d_m [\cos(\delta_m) J_{m+1}(k\rho) - \sin(\delta_m) Y_{m+1}(k\rho)] \begin{pmatrix} 1 \\ 0 \end{pmatrix}, \quad (\text{B14})$$

where Y_m are the Bessel functions of the second kind, $d_m(k)$ is a normalization constant and $\delta_m(k)$ is a scattering phase shift that determines the intensity of magnon scattering due to the presence of the skyrmion. The phase shifts can be calculated within the WKB approximation^{37,55} as

$$\delta_m(k) = \int_{\rho_1}^{\infty} d\rho \left(\sqrt{k^2 + \varepsilon_{\text{MS}} - U_{\text{WKB}}(\rho)} - k \right) d\rho + \frac{\pi}{2} |m+1| - k\rho_1, \quad (\text{B15})$$

where ρ_1 is the first classical turning point $\varepsilon_k = U_{\text{WKB}}(\rho_1)$, when approaching $U_{\text{WKB}}(\rho)$ from large distances. The effective WKB potential is given by

$$U_{\text{WKB}}(\rho) = \varepsilon_k - \frac{\mu(\rho/\rho_0)}{\rho^2}, \quad (\text{B16})$$

with $\rho_0 = \sqrt{2/(2\kappa + h)} = 1/\sqrt{\varepsilon_{\text{MS}}}$ and $\mu(x)$ is the eigenvalue of the operator

$$\Lambda(x) = -(m\mathbb{1} + \sigma_z)^2 + \rho_0^2 e^{2x} \left(-\frac{1}{\rho_0^2} \mathbb{1} + \varepsilon_k \sigma_z - \mathcal{V}_m^{\text{sc}}(\rho_0 e^x) \right), \quad (\text{B17})$$

which corresponds to the eigenvector $v(x) \propto \begin{pmatrix} 1 \\ 0 \end{pmatrix}$. Here, we use $x = \log(\rho/\rho_0)$ and $v(x) = \psi_m^{\text{sc}}(\rho_0 e^x)$. Taking into account the angular coordinate, scattering states are described by

$$\Psi_{m,k}^{\text{sc}}(\mathbf{r}) = \frac{e^{im\phi}}{\sqrt{2\pi}} \psi_{m,k}^{\text{sc}}(\rho), \quad (\text{B18})$$

where $\psi_{m,k}^{\text{sc}}(\rho)$ is given in Eq. (B14), while scattering phase shifts $\delta_m(k)$ are calculated with the help of Eq. (B15).

Appendix C: Technical Details on the Mass Tensor

In this Appendix we discuss various technical details relevant to the mass tensor \mathcal{M}_{ij}^0 and \mathcal{M}_{ij}^T .

First order perturbation theory for the calculation of mass term \mathcal{M}_{ij}^0 . To investigate the effect of the external perturbations to magnon modes it is convenient to consider small perturbations \mathcal{V} that alter the eigenfunctions $\tilde{\Psi}_n = \Psi_n + \delta\Psi_n$, where Ψ_n are eigenfunctions of the unperturbed Hamiltonian \mathcal{H} given in Eq. (B1). Since damping and mass depend on the

inverse of the magnon energy ε_n , we expect that bound states below the gap have a larger contribution to the mass terms \mathcal{M}_{xx}^0 and \mathcal{M}_{yy}^0 appearing in Eq. (31). Among them, the state Ψ_{-1} turns out to be the most important one for the form of external perturbations considered here. Under the assumption that we keep only the state Ψ_{-1} in the sum over all magnon modes we arrive at

$$\begin{aligned}\mathcal{M}_{xx}^0 &= I_1 + I_2 + I_3, \\ \mathcal{M}_{yy}^0 &= I_1 + I_2 - I_3,\end{aligned}\quad (C1)$$

where the integrals I_i are given by

$$\begin{aligned}I_1 &= \frac{\tilde{S}^2 N_A}{2\varepsilon_{-1}(\varepsilon_{-1}^0)^2} |\langle \Phi_{-1}, \mathcal{W}\Psi_{-1} \rangle|^2, \\ I_2 &= \frac{\tilde{S}^2 N_A}{2\varepsilon_{-1}(\varepsilon_{-1}^0)^2} |\langle \Psi_1, \mathcal{W}\Psi_{-1} \rangle|^2,\end{aligned}\quad (C2)$$

while I_3 contains contributions from both zero modes,

$$I_3 = \frac{\tilde{S}^2 N_A}{2\varepsilon_{-1}(\varepsilon_{-1}^0)^2} (\langle \Psi_1, \mathcal{W}\Psi_{-1} \rangle \langle \Psi_{-1}, \mathcal{W}\Phi_{-1} \rangle + \text{h.c.}). \quad (C3)$$

Off-diagonal elements $\mathcal{M}_{xy} = -\mathcal{M}_{yx} = iM_{xy}$ are equal to $M_{xy} = I_1 - I_2$, but they do not contribute to the equation of motion for the skyrmion center-of-mass \mathbf{R} . In the above expressions we have used the following exact relations,

$$f_x = -\frac{i}{\sqrt{2}} \sigma_z (\Psi_1 + \Phi_{-1}), \quad (C4)$$

$$f_y = -\frac{1}{\sqrt{2}} \sigma_z (\Psi_1 - \Phi_{-1}). \quad (C5)$$

The eigenstate Ψ_{-1} has been calculated variationally in Appendix B in the small-skyrmion limit. For this calculation, the skyrmionic static configuration is required, where we use solution (37) and (A5) for the angle $\Theta_0(\rho)$ for a given set of parameters κ and h . The skyrmion radius λ is determined by fitting the trial function (A5) to the one obtained numerically. For all external perturbations we have considered in Sec. IV, we find that $\mathcal{M}_{xx}^0 = \mathcal{M}_{yy}^0$, whenever \mathcal{V} is isotropic in \hat{x} and \hat{y} direction.

Finite temperature mass term \mathcal{M}_{ij}^T . From the angular dependence of the eigenstates $\Psi_n(\phi, \rho) = e^{im\phi} \psi_{n,m}(\rho)$ and the form of the operator Γ_i given in Eq. (10) we conclude that in the finite T expression of the mass Eq. (33) only states with angular momentum difference $\Delta m = \pm 1$ contribute. For the parameter range considered here we find two bound states below the continuum with $m = 0$ and $m = 2$. Since the zero mode $m = 1$ is excluded from summations, there are no bound-bound state contributions. To calculate the contribution from the scattering states, the sum over the quantum

number n in Eq. (33) is replaced by

$$\sum_n \Psi_n \rightarrow \sum_m \sum_k \Psi_{m,k}^{\text{sc}} \rightarrow \sum_m \left(\sum_k \Psi_{m,k}^{\text{free}} - \sum_k \Psi_{m,k}^{\text{sc}} \right), \quad (C6)$$

where we have subtracted background fluctuations described by Eq. (B12) in order to render the result finite in the thermodynamic limit. In addition, the discrete sum over k is replaced by $\sum_k \rightarrow \frac{L}{\pi} \int_0^\infty dk$.

Next, we consider the expression for $\mathcal{M}_{xx}^{\text{bs-sc}}$,

$$\mathcal{M}_{ii}^{\text{bs-sc}} = \sum_m \int_0^\infty dk k \frac{\mathcal{C}_{m,k}}{\tilde{\varepsilon}_m - \tilde{\varepsilon}_k} [\coth(\frac{\beta \tilde{\varepsilon}_k}{2}) - \coth(\frac{\beta \tilde{\varepsilon}_m}{2})], \quad (C7)$$

with elements $\mathcal{C}_{m,k} = \frac{1}{8} \tilde{c}_m^2 (g_{m,m-1} + g_{m,m+1})$, and

$$\begin{aligned}g_1^{m,m'} &= (1 - \cos(\delta_{m'}))^2 \left[\frac{a_m k}{2} (D_1^{m'} - D_1^{m'+2}) \right. \\ &\quad \left. + a_m m' D_2^{m'+1} + b_m D_3^{m'+1} \right]^2,\end{aligned}\quad (C8)$$

with integrals $D_1^m = (f_0 J_m)$, $D_2^m = (f_0 J_m / \rho)$ and $D_3^m = (f_0 J_m \Theta_0' \cot \Theta_0)$. We use $(\cdots) = \int_0^\infty \cdots d\rho \rho$. The normalization constant \tilde{c}_m is defined as

$$\tilde{c}_m(k) = \frac{\sqrt{L/\pi}}{\sqrt{\int_0^L d\rho \rho J_{m+1}^2(k\rho)}}, \quad (C9)$$

for a finite system size of area πL^2 . Note that we have neglected terms proportional to $\sin(\delta_m)$ under the assumption $\cos(\delta_m) \gg \sin(\delta_m)$. In Fig. 8 we present the magnetic field dependence of $\mathcal{M}_{ii}^{\text{bs-sc}}$ for $T = 0.2$ for a skyrmion with $\kappa = 0.1$, $S = 1$, $\tilde{J}/\tilde{D} = 4$ and $L \rightarrow \infty$. For this choice, we take into account two localized modes with energy less than ε_{MS} in the magnetic field region between $h = 0.34$, where the skyrmion energy becomes positive, up to $h = 0.42$ where the bound state energy passes into to the continuous spectrum (see Fig. 10 (b)). To calculate the contribution from the scattering states, we use the states $\Psi_{m,k}^{\text{sc}}$ given in Eq. (B14), and under the assumption that $\cos^2(\delta_m(k)) \gg \sin^2(\delta_m(k))$ we arrive at the following result,

$$\begin{aligned}\mathcal{M}_{ii}^{\text{sc}} &= \frac{1}{8} \sum_m \int_0^\infty dk \frac{\beta k^2 g_{m,m+1}}{\sinh^2(\beta \tilde{\varepsilon}_k/2)} \\ &+ \frac{1}{8} \sum_{m>0} \int_0^\infty k dk \int_k^\infty k' dk' \frac{C_{k,k'}(\beta)}{\tilde{\varepsilon}_k - \tilde{\varepsilon}_{k'}} (G_{m,m+1}^{k,k'} + G_{m,m-1}^{k,k'}),\end{aligned}\quad (C10)$$

with $g_{m,m'}^{k,k'} = \tilde{c}_m(k)^2 \tilde{c}_m(k')^2 [-\cos^2(\delta_m(k)) \cos^2(\delta_{m'}(k')) + 1]$, $C_{k,k'}(\beta) = [\coth(\beta \tilde{\varepsilon}_{k'}/2) - \coth(\beta \tilde{\varepsilon}_k/2)]$ and $G_{m,m'}^{k,k'} = g_{m,m'}^{k,k'} k^{(m+m'+1)} (k')^{-(m+m'+3)}$. In Fig. 9 we plot the temperature and magnetic field dependence of $\mathcal{M}_{ii}^{\text{sc}}$ for a skyrmion with $\kappa = 0.1$, $S = 1$, $\tilde{J}/\tilde{D} = 4$ and $L \rightarrow \infty$. Summations over quantum number m converge and are bounded between $-7 \leq m \leq 7$.

- ¹ Skyrme, T. H. R. Nucl. Phys. **31**, 556 (1962).
- ² U. K. Röbller, A. N. Bogdanov, and C. Pfeiderer, Nature **442**, 797 (2006).
- ³ S. Mühlbauer, B. Binz, F. Jonietz, C. Pfeiderer, A. Rosch, A. Neubauer, R. Georgii, and P. Böni, Science **323**, 915 (2009).
- ⁴ A. Neubauer, *et al.*, Phys. Rev. Lett. **102**, 186602 (2009).
- ⁵ C. Pappas, *et al.*, Phys. Rev. Lett. **102**, 197202 (2009).
- ⁶ F. Wilczek and A. Zee, Phys. Rev. Lett. **51**, 2250 (1983).
- ⁷ N. Papanicolaou and T.N. Tomaras, Nucl. Phys. **B360**, 425 (1991).
- ⁸ A. Fert, V. Cros, and J. Sampaio, Nat. Nanotechnol. **8**, 152 (2013).
- ⁹ N. S. Kiselev, A. N. Bogdanov, R. Schaefer, and U. K., J. Rössler, Phys. D **44**, 392001 (2011).
- ¹⁰ F. Jonietz, S. Mühlbauer, C. Pfeiderer, A. Neubauer, W. Münzer, A. Bauer, T. Adams, R. Georgii, P. Böni, R. A. Duine, K. Everschor, M. Garst, and A. Rosch, Science **330**, 1648 (2010).
- ¹¹ J. Iwasaki, M. Mochizuki, and N. Nagaosa, Nat. Comm. **4**, 1463 (2013).
- ¹² G. Yang, P. Stano, J. Klinovaja, and D. Loss, Phys. Rev. B. **93**, 224505 (2016).
- ¹³ C. Nayak, S. H. Simon, A. Stern, M. Freedman, and S. Das Sarma, Rev. Mod. Phys. **80**, 1083 (2008).
- ¹⁴ E. M. Lifshitz and L. P. Pitaevskii, *Statistical Physics, Part 2*, 3rd ed., Course of Theoretical Physics, Vol. 9 (Pergamon, Oxford, 1980).
- ¹⁵ T. L. Gilbert, IEEE Trans. Magn., **40**, 3443 (2004).
- ¹⁶ A. A. Thiele, Phys. Rev. Lett. **30**, 230 (1973).
- ¹⁷ M. Stone, Phys. Rev. B **53**, 16573 (1996).
- ¹⁸ C. Schütte, J. Iwasaki, A. Rosch, and N. Nagaosa, Phys. Rev. B **90**, 174434 (2014).
- ¹⁹ I. Makhfudz, B. Krüger, and O. Tchernyshyov, Phys. Rev. Lett. **109**, 217201 (2012).
- ²⁰ K. Everschor, M. Garst, B. Binz, F. Jonietz, S. Mühlbauer, C. Pfeiderer, and A. Rosch, Phys. Rev. B **86**, 054432 (2012).
- ²¹ J. Iwasaki, M. Mochizuki, and N. Nagaosa, Nat. Commun. **4**, 1463 (2013).
- ²² S. Heinze, K. von Bergmann, M. Menzel, J. Brede, A. Kubetzka, R. Wiesendanger, G. Bihlmayer, and S. Blügel, Nat. Physics **7**, 713 (2011).
- ²³ R. Wiesendanger, Nat. Reviews Materials **1**, 16044 (2016).
- ²⁴ C. Moreau-Luchaire, C. Moutas, N. Reyren, J. Sampaio, C. A. F. Vaz, N. Van Horne, K. Bouzehouane, K. Garcia, C. Deranlot, P. Warnicke, P. Wohlhueter, J.-M. George, M. Weigand, J. Raabe, V. Cros, and A. Fert, Nat. Nanotechnol. **11**, 444 (2016).
- ²⁵ S. Woo, K. Litzius, B. Krüger, M.-Y. Im, L. Caretta, K. Richter, M. Mann, A. Krone, R. M. Reeve, M. Weigand, P. Agrawal, I. Lemesch, M.-A. Mawass, P. Fischer, M. Kläui, and G. S. D. Beach, Nat. Mater. **15**, 501 (2016).
- ²⁶ A. Roldán-Molina, M. J. Santander, A. S. Nunez, and J. Fernández-Rossier, Phys. Rev. B **92**, 245436 (2015).
- ²⁷ J. L. Gevais and B. Sakita, Phys. Rev. D **11**, 2943 (1975).
- ²⁸ J. L. Gevais, A. Jevicki, and B. Sakita, Phys. Rev. D **12**, 1038 (1975).
- ²⁹ B. Sakita, *Quantum Theory of Many Variable Systems and Fields*, World Scientific, Singapore 1985.
- ³⁰ R. Rajaman, *Solitons and Instantons: An Introduction to Solitons and Instantons in Quantum Field Theory*, North Holland, 1982.
- ³¹ H-B. Braun and D. Loss, Phys. Rev. B **53**, 3237 (1996).
- ³² J. Kyriakidis, D. Loss, and A. H. MacDonald, Phys. Rev. Lett. **83**, 1411 (1999).
- ³³ X. Zhang, M. Ezawa, and Y. Zhou, Sci. Rep. **5**, 9400 (2015).
- ³⁴ Y. Zhou and M. Ezawa, Nat. Commun. **5**, 4652 (2014).
- ³⁵ D. D. Sheka, I. A. Yastremsky, B. A. Ivanov, G. M. Wysin, and F. G. Mertens, Phys. Rev. B **69**, 054429 (2004).
- ³⁶ *Quantum Dissipative Systems*, U. Weiss, Series in Modern Condensed Matter, Vol. 10, World Scientific (1999).
- ³⁷ C. Schütte and M. Garst, Phys. Rev. B **90**, 094423 (2014).
- ³⁸ S. Schroeter, M. Garst, and A. Rosch, *Skymion caloritronics in chiral magnets*, manuscript in preparation.
- ³⁹ F. Büttner, C. Moutafis, M. Schneider, B. Krüger, C. M. Günther, J. Geilhufe, C. v. Korff Schmising, J. Mohanty, B. Pfau, S. Schaffert, A. Bisig, M. Foerster, T. Schulz, C. A. F. Vaz, J. H. Franken, H. J. M. Swagten, M. Kläui, and S. Eisebitt, Nat. Phys. **11**, 225 (2015).
- ⁴⁰ J. R. Cash and F. Mazzia, J. Comput. Appl. Math. **184**, 362 (2005).
- ⁴¹ S. Lin, C. D. Batista, and A. Saxena, Phys. Rev. B **89**, 024415 (2014).
- ⁴² S. Li and L. N. Bulavskii, Phys. Rev. B **88**, 060404(R) (2013).
- ⁴³ D. D. Sheka, B. A. Ivanov, and F. G. Mertens, Phys. Rev. B, **64**, 024432 (2001).
- ⁴⁴ A. Mehlin, F. Xue, D. Liang, H. F. Du, M. J. Stolt, S. Jin, M. L. Tian, and M. Poggio, Nano Letters **15**, 4839 (2015).
- ⁴⁵ X. Z. Yu, N. Kanazawa, Y. Onose, K. Kimoto, W. Z. Zhang, S. Ishiwata, Y. Matsui, and Y. Tokura, Nat. Mater. **10**, 106 (2011).
- ⁴⁶ S. Seki, X. Z. Yu, S. Ishiwata, and Y. Tokura, Science **336**, 198 (2012).
- ⁴⁷ T. Adams, A. Chacon, M. Wagner, A. Bauer, G. Brandl, B. Pedersen, H. Berger, P. Lemmens, and C. Pfeiderer, Phys. Rev. Lett. **108**, 237204 (2012).
- ⁴⁸ O. Janson, I. Rousochatzakis, A. A. Tsirlin, M. Belesi, A. A. Leonov, U. K. Röbller, J. van den Brink, and H. Rosner, Nat. Comm. **5**, 5376 (2014).
- ⁴⁹ J. Iwasaki, W. Koshibae, and N. Nagaosa, NanoLett. **14**, 4432 (2014).
- ⁵⁰ A. B. Butenko, A. A. Leonov, U. K. Röbller, and A. N. Bogdanov, Phys. Rev. B **82**, 052403 (2010).
- ⁵¹ N. Bogdanov and A. Hubert, J. Magn. Magn. Mater **138**, 255 (1994).
- ⁵² M. N. Wilson, A. B. Butenko, A. N. Bogdanov, and T. L. Monch- esky, Phys. Rev. B **89**, 094411 (2014).
- ⁵³ S. Banerjee, J. Rowland, O. Erten, and M. Randeria, Phys. Rev. X **4**, 031045 (2014).
- ⁵⁴ B. A. Ivanov and D. D. Sheka, JETP **82**, 436 (2005).
- ⁵⁵ M. V. Berry and K. E. Mount, Rep. Prog. Phys. **35**, 315 (1972).
- ⁵⁶ H. B. Braun, J. Kyriakidis, and D. Loss, Phys. Rev. B **56**, 8129 (1997).
- ⁵⁷ J. Brooke, T. F. Rosenbaum, and G. Aeppli, Nature **413**, 610 (2001).